Wavefront Sensor and Deformable

Mirror Design Parameters for GNAO

GNAO-SYS-SIM-004

Related PBS ID: 5.2

M. van Dam, G. Sivo, E. Marin

April 29, 2020

Contents

Document Acceptance and Release Notice

This document is a managed document. To identify changes, each page contains a release number and a page number. This document is authorized for release once all signatures have been obtained.

APPROVED:	*Approval on file* William Rambold GNAO Project Lead Systems Engineer	Date:	2020-11-12
APPROVED:	*Approval on file* Manuel Lazo GNAO Project Manager	Date:	2020-11-12
APPROVED:	*Approval on file* Gaetano Sivo GNAO Principal Investigator	Date:	2020-11-12
APPROVED:	*Approval on file* Henry Roe GNAO Sponsor, Gemini Deputy Director	Date:	2020-11-12

Change Record

| Version	Date	Description	Owner Name	Change Request
3.0	2020-11-12	Released through formal change control process	M. van Dam	GEM-189

1 Introduction

The Gemini North Adaptive Optics (GNAO) instrument is a next generation multi-conjugate adaptive optics (MCAO) system designed for a wide range of science cases. The aim is to produce near diffraction-limited image quality for J-, H- and K-bands.

The simulated performance of GNAO was first investigated in a document titled "Simulated Performance of GNAO".[1] The results were used to inform the Conceptual Design, which was reviewed in September 2019. Following the review, significant changes were made to the baseline architecture and there were also a few changes to the modeling and simulation parameters, all of which are recorded in the Appendix (Section 24).

In this report, we use simulations and semi-analytical calculations to evaluate the performance of the finer details of the new design. especially the aspects that were not well addressed at the Conceptual Design level.

The design investigated in this report has three deformable mirrors (DMs) at three conjugate altitudes and a dedicated tip-tilt mirror. Two lasers are used to produce five side-launched laser guide stars (LGSs), as shown in Figure 1. This configuration has been shown to produce the best performance.[2]
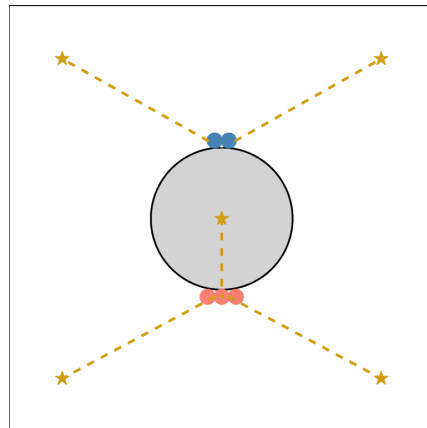
Figure 1: The launch configuration used in this report. The colors of the launch telescope (blue and salmon) represent which of the two lasers is producing the laser light launched by the corresponding launch telescope.

The wavefront is measured with five laser guide star wavefront sensors (LGS WFSs). LGS-based AO systems also require natural guide stars (NGSs) to measure tip-tilt and focus. The baseline design for GNAO uses three NGSs to measure tip-tilt over the science field of view. Using more NGSs can be helpful if the NGSs are available. A slow focus sensor guides on one of the NGSs to measure the variations in the altitude of the sodium layer, as well as any quasi-static low-order aberrations induced by the LGS elongations.

---

[1]Marcos van Dam, Gaetano Sivo and Eduardo Marin, "Simulated Performance of GNAO," GNAO-SYS-SIM-001, v3.1: 22 October 2019

[2]Marcos van Dam, Eduardo Marin, Gaetano Sivo, "GNAO Laser Launch Telescope Location," v1.0, GNAO-SYS-SIM-003, 11 November 2019

2 Simulation description and simulation parameters

In this section, we describe the simulation tool as well as the inputs to the simulations.

2.1 Simulation tool

End-to-end Monte-Carlo simulations were run using YAO,[3-4] an open-source, user-configurable code written in the yorick language, along with custom scripts and parameter files. This code has over 100 users and has been used extensively to design and operate GeMS, the Gemini South MCAO system.

Some modifications to the YAO code base were made to support specific features needed for this work, and these changes have been released for general use. In particular, Rayleigh contamination from off-axis launch locations was implemented, along with automatic subaperture selection based on the ratio between the Rayleigh backscatter and the sodium return.

The control law used in the simulations is very simple. The high-order loop uses a leaky integrator with a loop gain of 0.4 and a leak of 0.01. The tip-tilt loop also has a gain of 0.4, while the up-link tip-tilt loop has a gain of 0.1. A more sophisticated approach is needed to improve the tip-tilt performance, but the implementation of such a controller is beyond the scope of this report. In all cases, the loop delay was one frame.

Tomographic wavefront reconstructors for MCAO are not fully implemented in YAO. The wavefront reconstructors are hand-coded using a custom yorick script. A description of the high-order wavefront tomographic reconstructor is presented in Section 25, while the tip-tilt tomographic reconstructor is described in 25.

2.2 Atmospheric parameters

The atmospheric profile used in the simulations represent the median Mauna Kea conditions sourced from the TMT (Table 1). The outer scale is 30 m. Random wind directions were applied to the measured wind speeds.

Elevation (m)	0	500	1000	2000	4000	8000	16000
Wind speed (m/s)	5.6	5.77	6.25	7.57	13.31	19.06	12.14
Wind direction (°)	190	255	270	350	17	29	66
Turbulence fraction	0.4557	0.1295	0.0442	0.0506	0.1167	0.0926	0.1107

Table 1: Turbulence profile used for Mauna Kea 50th percentiles. The value of r_0 at a wavelength of 500 nm is 0.186 m.

2.3 Sodium return and Rayleigh

The simulations in this report assume the use of two Toptica 20 W lasers, one of which are split into two and three LGS beams respectively (see Figure 2). The return at the top of the telescope from a single laser pointed at zenith is 6.85 Mph m^{-2} s^{-1}. As a comparison, Holzlöhner and predicts a return of 14 Mph $m^{-2}s^{-1}$ at the optimal pointing direction with a 20 W TOPTICA laser of which 16 W are launched, at the Maunakea site with atmospheric transmission of 0.84,[5] using a sodium density for

---

[3]Rigaut, François, and Marcos van Dam. "Simulating astronomical adaptive optics systems using Yao." AO4ELT (2013).

[4]http://frigaut.github.io/yao/

[5]Holzlöhner R. et al., "Optimization of CW Sodium Laser Guide Star Efficiency," A&A 510, 0004-6361 January, (2016).

this calculation is 3.75×10^{13} atoms m^{-2}. The sodium return in these simulations is assumed to be proportional to the cosine of the zenith angle.

The Rayleigh contamination (called fratricide) for the side-launched laser configuration used in this report is plotted in Figure 2. The impacted subapertures are masked out and not used in the reconstruction process.
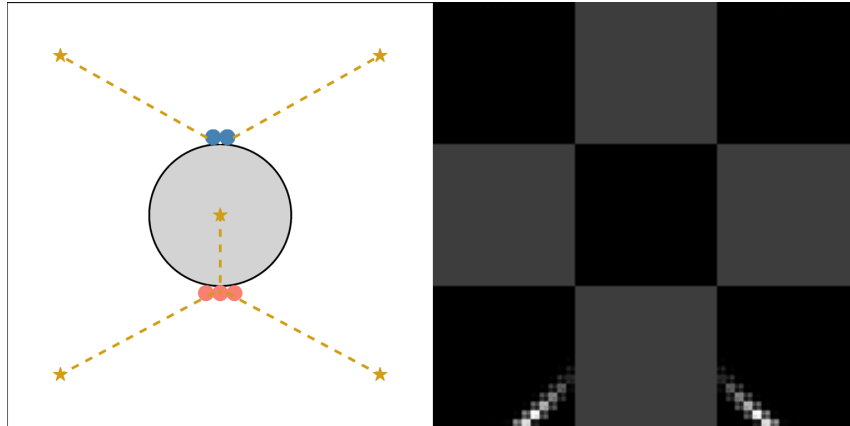
Figure 2: Launch configuration (left) and corresponding Rayleigh contamination for each of the five LGS WFSs (right). The colors of the launch telescope (blue and salmon) represent which of the two lasers is producing the laser light launched by the corresponding launch telescope.

2.4 Guide star locations

There are five LGSs, located at [0", 0"], [-35", -35"], [-35", 35"], [35", -35"] and [35", 35"], while three NGSs are located at [0", 35"], [40", -30"] and [-40", -20"].

2.5 Optical throughput

The optical throughput of the atmosphere is 0.89, the telescope is 0.821, and GNAO is 0.3, for a total of 0.22.

2.6 LGS WFS camera

The baseline camera for the LGS WFS is an OCAM2 camera by First Light Imaging. While other suitable options exist (especially low read noise cameras developed by the MIT Lincoln Laboratory), the OCAM2 camera is a commercially available off-the-shelf product with numerous users, so it is a low risk option. The OCAM2 camera is based on the CCD220, a 240x240 pixel detector. This is CCD uses electron multiplication, which allows us to get subelectron read noise. The penalty to be paid is the increase in the excess noise factor from 1 to 1.41, which is equivalent to reducing the quantum efficiency of the detector by a factor of 2. The properties of the OCAM2 are tabulated in Table 2. The read noise of OCAM2 can be reduced by increasing the multiplication gain, but this ages the camera faster and should be avoided.

Camera	OCAM2
Pixels	240x240
Excess noise	1.41
Quantum efficiency @589 nm	0.90
Read noise	0.5 e-
Dark current	10 e-/s
Charge diffusion FWHM	0.5 pixels (?)

Table 2: Properties of OCAM2 wavefront sensing cameras, obtained from Feautrier *et al*.[6] The question marks indicates an educated guess.

2.7 NGS WFS Camera

An NGS is needed to measure tip-tilt across the field, focus and LGS aberrations.[7] The tip-tilt and tip-tilt a measurement is made at a frame rate of 100 Hz or more using three tip-tilt stars, while the focus measurement can be made at a much slower rate (at least one measurement every 30s). The focus and truth sensor has not yet been defined. Three options are being considered for the pick-off, which affect the throughput to the NGS sensor. A beamsplitter that splits light across the full field between the two sensors, a pick-off mirror that sends all the light from one star to the truth sensor, and a pick-off dichroic that sends part of the light from the brightest star to the truth sensor. We will assume that 90% of the light across the full field is sent to the tip-tilt sensor, so the total throughput is 0.22x0.90 = 0.20.

The tip-tilt sensing camera mirrors the NGS2 tip-tilt sensor to be inserted on Canopus in July 2019. The noise characteristics are tabulated in Table 3. The read noise is 300 / EM gain. The read noise can be reduced to less than 0.1 e- using a higher electron multiplication gain, which stresses and ages the camera. There is an additional limitation in the NGS2 sensor: the full well is 800 kiloelectrons / EM gain. The EM gain needs to be set so that the brightest star does not saturate, which will not be optimal for the faintest stars. We ignore this limitation in this report, and note that there are other alternative cameras, such as the C-MORE camera from First Light Imaging and the Andor Zyla 4.2.

[6]Feautrier, Philippe, et al. "Characterization of OCam and CCD220: the fastest and most sensitive camera to date for AO wavefront sensing." Adaptive Optics Systems II. Vol. 7736. International Society for Optics and Photonics, 2010.

[7]Clare, Richard M., Marcos A. van Dam, and Antonin H. Bouchez. "Modeling low order aberrations in laser guide star adaptive optics systems." Optics express 15.8 (2007): 4711-4725.

Camera	CCD
Pixels	512x512
Maximum frame rate[8]	800 Hz
Excess noise	1.41
Quantum efficiency VRI-bands[9]	0.80
Read noise	0.5 e-
Dark current[8]	0.00058 e-/s
Charge diffusion FWHM	0.25 pixels

Table 3: Properties of the NGS2 wavefront sensing camera.

The quantum efficiency as a function of wavelength is plotted in Figure 3. If we pass the same wavelength range as NGS2 (450-950 nm), the photometric parameters are presented in Table 4.
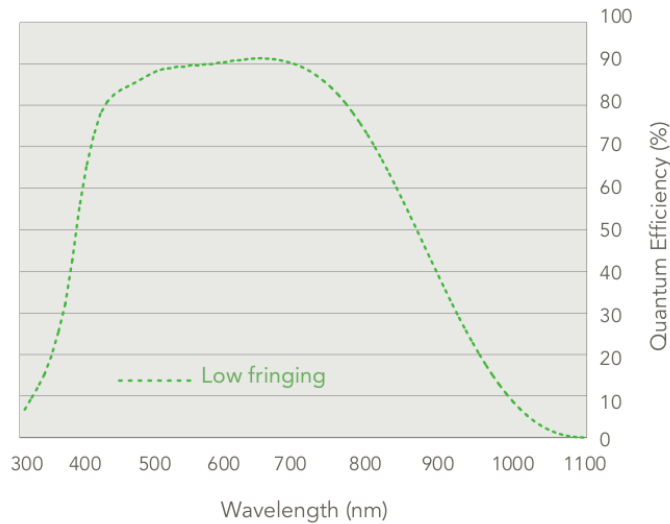
Figure 3: Quantum efficiency as a function of wavelength for the Nuvu Nnu512 IS camera.

Parameter	Value
Passband	450 - 950 nm
Photometric zero point (photons / second)	1.30e12
Sky background (magnitude / arcsec^2)	18.5

Table 4: Photometric parameters used in the simulations.

The NGS2 system for GeMS allows only a single frame rate to be used for all ROIs. Correia *et al* found no benefit to running some tip-tilt sensors faster than others for MCAO.[10] However, intuitively it would seem that having one tip-tilt sensor running faster should reduce the effect of vibration. We defer consideration of a multi-frame rate system until later.

---

[8]Rigaut, François, et al. "NGS2: a focal plane array upgrade for the GeMS multiple tip-tilt wavefront sensor." Adaptive Optics Systems V. Vol. 9909. International Society for Optics and Photonics, 2016.

[9]http://www.nuvucameras.com/wp-content/uploads/2018/02/NuvuCameras-HNu512_IS.pdf

[10]Correia, Carlos, et al. "Increased sky coverage with optimal correction of tilt and tilt-anisoplanatism modes in laser-guide-star multiconjugate adaptive optics." JOSA A 30.4 (2013): 604-615.

2.8 Science metrics

The image quality metrics calculated by by default are the Strehl ratio, the Full Width at Half Maximum (FWHM), and the 50% encircled energy diameter. Other image quality metrics can also be computed if desired. The wavelengths of interest are 1.25, 1.65, 2.2 microns, which corresponds approximately to the central wavelengths of J-, H-, and K-bands. The target locations are in a regular grid with positions [-47.4", -31.6", -15.8", 0", 15.8", 31.6", 47.4"] in both x and y, over a circle with a diameter of 2', as shown in Figure 4.
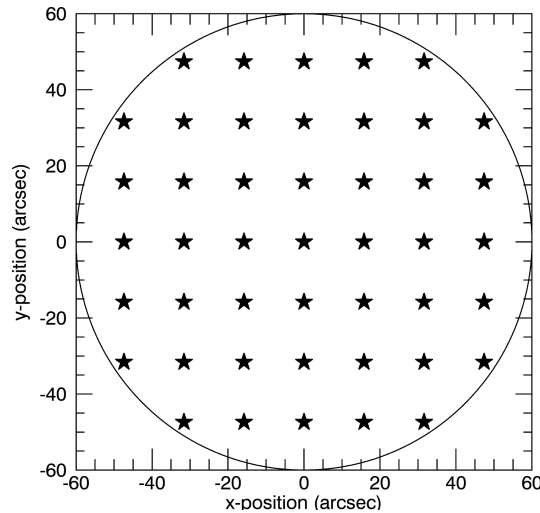
Figure 4: Location of science targets used to optimize the wavefront correction and to evaluate the image quality delivered by GNAO.

3 LGS wavefront sensor parameters

3.1 Number of subapertures

The number of subapertures is typically tightly coupled with the number of actuators in the ground layer DM. However, we also need to consider the performance if an adaptive secondary mirror (ASM) is installed on the telescope. This upgrade is under consideration but is not part of the GNAO project. Increasing the number of subapertures will benefit the on-axis case in particular. The trade-off is that a larger number of subapertures results in more measurement noise, and also requires more computing power.

Let us consider where the AO system corrects the wavefront along the optical axis of the telescope. For simplicity, we consider that the number of DM actuators across the telescope pupil is equal to the number of lenslets across the pupil plus one, in what is known as the Fried configuration.

The performance as a function number of subapertures and sodium return is tabulated in Table 5. On-axis performance is optimized with 26x26 subapertures and "satisficed" with 20x20 subapertures. The exact number depends on the DM chosen.

Percentage sodium return	100%	50%	25%	12.5%
16x16 subapertures	0.719	0.703	0.675	0.621
22x22 subapertures	0.738	0.713	0.672	0.598
26x26 subapertures	0.747	0.722	0.671	0.593
32x32 subapertures	0.737	0.706	0.649	0.561

Table 5: On-axis K-band Strehl ratio as a function of number of subapertures and as a function of the reduction in sodium return from the nominal value at zenith.

3.2 Plate scale

The angular extent of each pixel, called the plate scale, is a critical parameter for a number of reasons. If the plate scale is too large, then the spots on the WFS are undersampled, and there is a non-linear relationship between displacement of the spot and the centroid. If the plate scale is too small, the measurement is noisier and we risk truncating the LGS spot if there are insufficient pixels in each subaperture.

The LGS spot size on the WFS depends on the factors recorded in Table 6.

	Expression	Typical value	Minimum	Maximum
Diffraction	$0.0152\,N_s$	0.24	0.24	0.48
Intrinsic LGS spot size		1.00	0.50	1.50
Launch telescope optics		0.50	0.50	0.50
Seeing (uplink and downlink)	$1.41\,r_0$	0.90	0.60	1.80
Charge diffusion	$0.3\,p_s$	0.30	0.20	0.50
LGS elongation	$206265\,dth^{-2}\cos(\zeta)$		0.00	2.44
Total			0.98	3.49

Table 6: Contributors towards the LGS spot size

N_s is the number of subapertures
r_0 is the Fried's parameter
p_s is the plate scale
d is the distance between the launch telescope and the subaperture
t is the thickness of the sodium layer
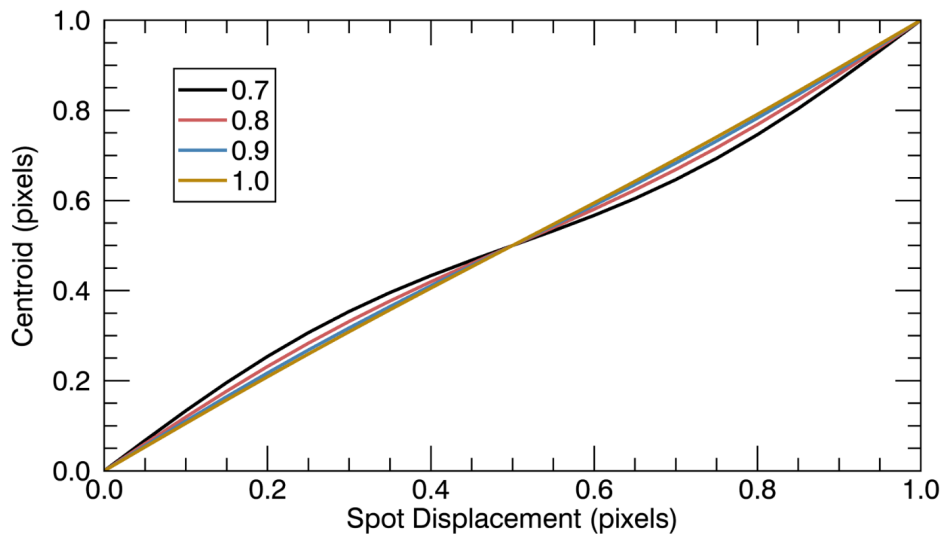h is the height of the sodium layer
t is the thickness of the sodium layer
ζ is the zenith angle

The important points from the table is that there is no scenario in which the LGS spot size will be less than 1" on the WFS. The maximally elongated spots will have a FWHM of around 3.5".

Figure 5: Centroid response due to a spot displacement as a function of FWHM in pixel units

Figure 5 plots the error due to pixelation as a function of the FWHM of the spot (in pixels). For a FWHM equal in size to the spot, or even slightly smaller, there is a linear response to the spot displacement. This conclusion is also reached by Thomas *et al*.[11] We conclude that the plate scale should be between 0.9" and 1.2", with a recommended value of 1.0", which is the value that has been used in the simulations to date.

As a comparison, we note that the Keck Observatory initially used quad cells with 2x2 2.4" pixels,[12] and this resulted in spot truncation and significant LGS induced aberrations due to the side launch.[13] The WFSs were upgraded to have 3.2" pixels, with a significant reduction in LGS aberrations.[14] The ESO VLT launches four LGSs from the side of the telescope. There are 6x6 pixels per subaperture with a pixel scale of 0.83".[15] The unelongated LGS spot size typically exhibits a FWHM of 1.5", hence it is well sampled with almost two pixels per FWHM. The typical spot elongation is 2.5" for the subaperture furthest from the launch telescope.

The minimum number of pixels required is 6x6 pixels per subaperture. Using more pixels increases the dynamic range, for a number of reasons:
- to accommodate for non-common path aberrations
- to loosen requirements on the performance of the up-link tip-tilt system
- ease of LGS acquisition

Therefore, I recommend 8x8 or more pixels per subaperture.

3.3 Field stop size

The function of the field stop is to prevent light from one subaperture leaking to the neighboring subaperture. The size of the field stop should correspond to the size of the subaperture. For an 8x8 subaperture with 1" pixels, the field stop should be a square with 8" sides.

3.4 Radial distance of the LGS constellation
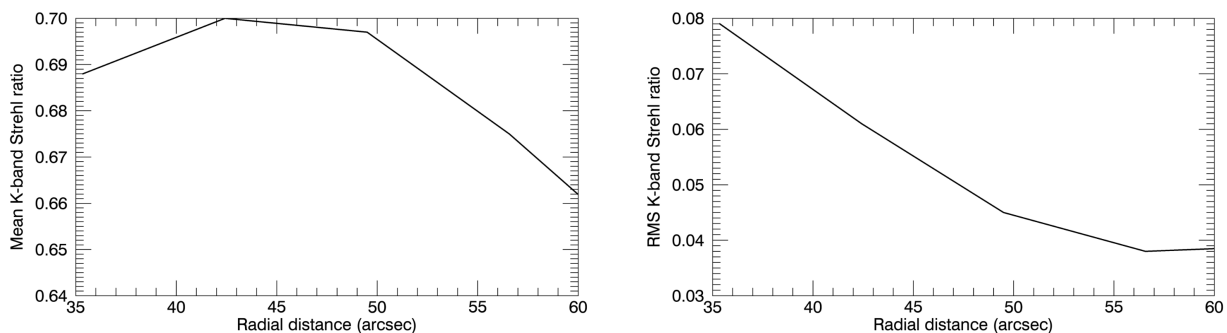
Figure 6: Mean K-band Strehl ratio (left) and variation across the field (right) as a function of radial distance of the outer guide stars at zenith.

[11] Oberti, Sylvain, et al. "The AO in AOF." Adaptive Optics Systems VI. Vol. 10703. International Society for Optics and Photonics, 2018.

[12] van Dam, Marcos A., David Le Mignant, and Bruce A. Macintosh. "Performance of the Keck Observatory adaptive-optics system." Applied Optics 43.29 (2004): 5458-5467.

[13] Clare, Richard M., Marcos A. van Dam, and Antonin H. Bouchez. "Modeling low order aberrations in laser guide star adaptive optics systems." Optics express 15.8 (2007): 4711-4725.

[14] Johansson, Erik M., et al. "Upgrading the Keck AO wavefront controllers." Adaptive Optics Systems. Vol. 7015. International Society for Optics and Photonics, 2008.

[15] Oberti, Sylvain, et al. "The AO in AOF." Adaptive Optics Systems VI. Vol. 10703. International Society for Optics and Photonics, 2018.

Figure 6 plots the Strehl ratio as a function of the location of the LGSs. The best Strehl ratio is obtained with the outer stars at [±30",±30"] (plotted as 42.4"), but the image quality is more constant across the field when the stars are further out. A good compromise is having the stars at [±35",±35"] (plotted as 49.5"),

4 Deformable mirror parameters

4.1 Conjugate altitude

The conjugate altitude was investigated using simulations and semi-analytical calculations in Reference 1. Here, we repeat the semi-analytical calculations in a more systematic way. We use the vertical distribution of turbulence tabulated in Table 7. The upper two layers have been subdivided into three layers each.

Elevation (km)	0	0.5	1	2	4	6	8	10	12	16	20
Wind speed (m/s)	5.6	5.8	6.25	7.57	13.31	19.1	19.1	19.1	12.1	12.1	12.1
Wind direction (°)	190	255	270	350	17	29	29	29	66	66	66
Turbulence fraction	0.456	0.130	0.044	0.051	0.117	0.031	0.031	0.031	0.037	0.037	0.037

Table 7: Turbulence profile used for the DM conjugate altitude simulations. The profile corresponds to the Mauna Kea 50th percentile with $r_0 = 0.186$ m. The upper two layers have each been subdivided into three layers.

One DM is conjugate to the ground, while the other two have varying altitudes. In all cases, the DM interactuator spacing is 50 cm. The generalized fitting error is calculated for zenith angles varying between 0° and 60°. The RSS generalized fitting error is presented in Tables 8 to 12.

DM3 altitude (km)

DM2 altitude (km)	8	9	10	11	12	13	14	15	16
3	159	154	150	147	144	142	140	139	137
4	155	151	147	143	140	138	136	134	133
5	155	151	147	144	141	139	137	135	134
6	155	152	149	146	144	142	140	138	137
7	155	152	150	147	146	144	143	141	139

Table 8: RSS generalized fitting error as a function of DM2 and DM3 altitude at zenith.

		DM3 altitude (km)								
		8	9	10	11	12	13	14	15	16
DM2 altitude (km)	3	167	163	158	154	151	148	147	145	144
	4	163	159	154	150	147	144	142	140	138
	5	162	158	154	150	147	144	142	140	138
	6	162	158	155	152	149	147	145	143	141
	7	162	158	156	153	151	149	148	146	143

Table 9: RSS generalized fitting error as a function of DM2 and DM3 altitude at a zenith. angle of 15°

		DM3 altitude (km)								
		8	9	10	11	12	13	14	15	16
DM2 altitude (km)	3	195	189	184	179	174	170	168	166	165
	4	190	184	179	174	169	165	162	160	158
	5	186	181	176	171	167	162	160	158	156
	6	185	181	177	173	169	165	162	160	158
	7	185	180	177	174	170	167	165	163	162

Table 10: RSS generalized fitting error as a function of DM2 and DM3 altitude at a zenith angle of 30°

		DM3 altitude (km)								
		8	9	10	11	12	13	14	15	16
DM2 altitude (km)	3	250	245	240	235	229	223	218	214	210
	4	246	241	236	230	224	218	213	208	204
	5	240	235	230	223	218	212	207	201	198
	6	236	231	225	220	214	209	204	199	195
	7	235	229	225	220	215	210	206	201	197

Table 11: RSS generalized fitting error as a function of DM2 and DM3 altitude at a zenith angle of 45°

		DM3 altitude (km)								
		8	9	10	11	12	13	14	15	16
DM2 altitude (km)	3	361	357	355	351	347	342	338	333	327
	4	357	353	350	347	343	338	334	328	323
	5	353	350	348	344	339	335	330	325	319
	6	349	346	343	339	334	330	324	319	313
	7	347	342	337	332	327	323	318	312	306

Table 12: RSS generalized fitting error as a function of DM2 and DM3 altitude at a zenith angle of 60°.

The outcome of the calculations is that for the turbulence profile modeled, the optimum configuration is DM2 at 5 or 6 km and DM3 at 16 km or higher. For reasons explained below, it may be preferable to lower the DM altitudes, in which case, placing DM2 at 5 km is preferable and having DM3 between 12 and 16 km is acceptable.

The strength of the turbulence does not affect the conclusions, since the error depends linearly on the wavefront, but the results also depend on the distribution of turbulence. The maximum wavefront error is minimized with the same configurations that minimize the average wavefront.

There are other considerations used to specify the altitude of the DMs, and these are discussed here.

- The optical design and the space envelope constrain the altitude of the DMs.
- The size of the metapupil (the footprint of the laser guide stars and the science field of view projected on the DM) depends on the DM altitude. A lower altitude for the high-altitude DM means that the metapupil is smaller, so a lower number of actuators is needed.
- The high altitude DM displaces and distorts the pupil seen by the WFSs. Reducing the altitude reduces the distortion of the pupil. Note that this effect is not modeled by YAO, so we have not yet been able to quantify it.
- The stroke needed to correct the plate scale modes in inversely proportional to the DM altitude.

4.2 Number of actuators

The number of DM actuators depends on the DM altitude and the DM pitch (interactuator spacing). The smaller the pitch, the better the performance, although the dependency is not very strong. Based on the results in Tables 13 to 14, a DM2 pitch of ≤0.8 m and a DM pitch of ≤1.2 m is proposed. For DMs at 0 km, 5 km and 12 km, this represents 21x21, 14x14 and 13x13 actuators across the metal pupil, or approximately 349, 156 and 137 actuators.

	DM3 pitch (m)			
	0.6	0.9	1.2	1.5
DM2 pitch (m) 0.4	137	139	142	146
0.6	138	140	144	147
0.8	141	143	146	150
1.0	143	145	148	152

Table 13: RSS generalized fitting error as a function of the pitch of DM2 (at 5 km) and DM3 (at 12 km) at zenith. The DM1 pitch is 0.4 m.

	DM3 pitch (m)			
	0.6	0.9	1.2	1.5
DM2 pitch (m) 0.4	214	216	219	223
0.6	216	217	220	224
0.8	218	220	223	227
1.0	221	223	226	230

Table 14: RSS generalized fitting error as a function of the pitch of DM2 (at 5 km) and DM3 (at 12 km) at a zenith angle of 45°. The DM1 pitch is 0.4 m.

We calculate the generalized fitting error for a DM configuration with DM altitudes of 0 km, 5 km and 14 km, with pitches of 0.4 m, 0.6 m and 0.9 m. The results are tabulated in Table 15, with the corresponding contour plots for zenith angles of 0° and 45° in Figure 7.

Zenith angle	RSS	Min	Max
0°	136	121	155
15°	141	126	161
30°	159	144	181
45°	207	189	245
60°	330	298	379

Table 15: RSS, minimum and maximum generalized fitting error (nm) across the field as a function of zenith angle.
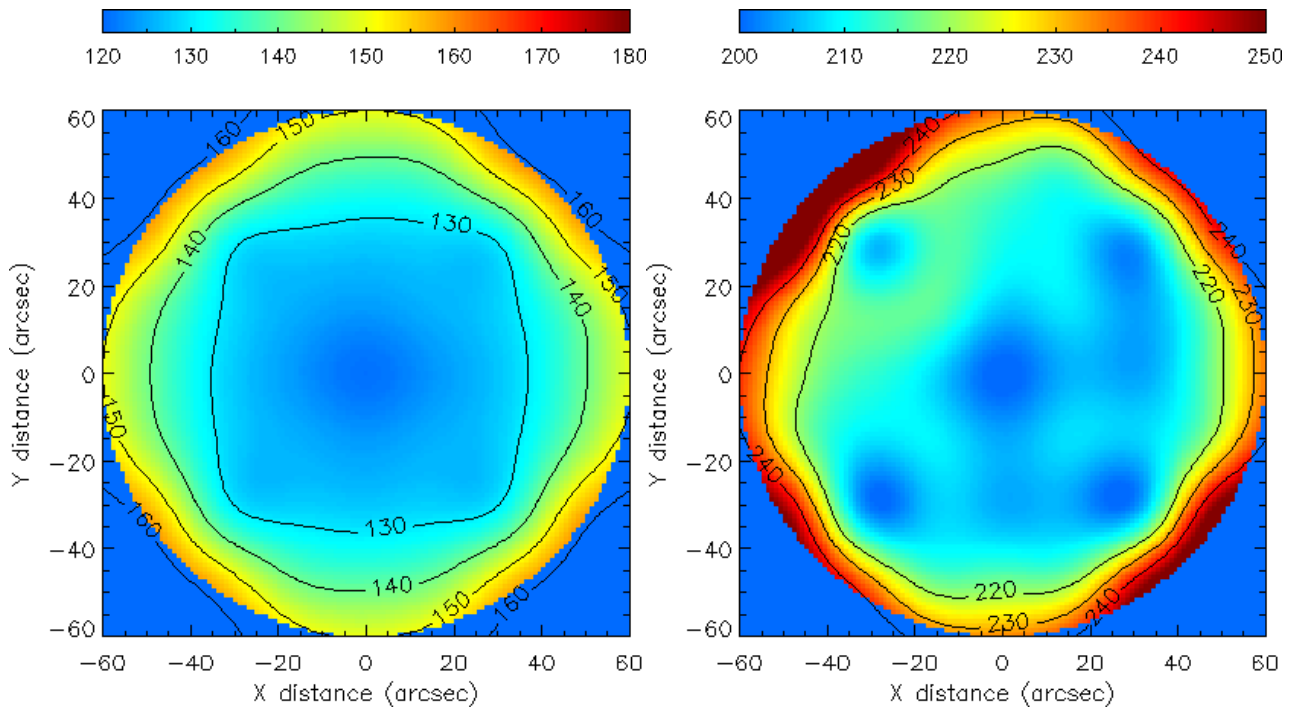
Figure 7: Generalized fitting error for DM altitudes of 0 k, 5 km and 14 km with pitches of 0.4 m, 0.6 m and 0.9 m respectively. The telescope is pointing at zenith (left) and at a 45° zenith angle (right).

Calculations were run to see how the number of DM1 actuators affects the wide-field performance. The results in Table 16 show that the wide field performance is sensitive to DM1 pitch.

DM1 pitch (m)				
0.30	0.40	0.49	0.59	0.71
132	136	140	146	152

Table 16: RSS generalized fitting error as a function of the pitch of DM1 (at 0 km). The DM1 pitch is 0.4 m. The DM2 and 3 pitches are 0.6 m and 0.9 m respectively.

4.3 Stroke

The DMs need to correct the atmospheric turbulence, telescope aberrations, wavefront aberrations induced by the AO system (including flattening the DM) and wavefront aberrations associated with the science instruments. In particular, we note that:

- DM1: must be able handle <u>all</u> of the atmospheric turbulence for GLAO/LTAO correction and the bulk of the non-common path aberrations.
- DM2: corrects only mid-layers
- DM3: corrects high altitude turbulence plus plate scale modes

Following the convention used in the ALPAO data sheets, we define the stroke of the DMs as the peak-to-valley value of the wavefront (the wavefront is twice the value of the mechanical deformation).

To specify DM1, simulations were run with a conventional NGS AO system for simplicity. The AO system has a DM with 17x17 actuators across the pupil and, optionally, a tip-tilt mirror. We report the K-band Strehl ratio as a function of DM stroke for an observation at zenith with an value of r_0 of 0.06 m (Table 17).

Stroke (µm)	2	3	4	5	6	7	8	9	10
With tip-tilt mirror	0.193	0.362	0.480	0.546	0.580	0.592	0.594	0.594	0.594
No tip-tilt mirror	0.107	0.251	0.387	0.475	0.539	0.573	0.585	0.588	0.589

Table 17: K-band Strehl ratio as a function of DM stroke (peak-to-valley wavefront) with and without a dedicated tip-tilt mirror.

Allowing for 2 µm of stroke to correct any static aberrations leads to the requirement that DM1 must have a stroke of 8 µm, with a goal of 10 µm. The ALPAO DMs appear to have easily enough stroke, including the ability to correct tip-tilt without a separate tip-tilt mirror. For example, the DM 468 can produce 12 µm of tip-tilt correction, 10 microns of µm, and 5 µm of interactuator difference.[16] An interesting option, however, would be to use the ALPAO DM241 and remove the tip-tilt mirror from the AOS. This DM has a maximum tip-tilt stroke of 40 µm, which corresponds to a tip-tilt ±1", certainly sufficient to correct for atmospheric tip-tilt and more than likely sufficient to correct the telescope contribution as well.

The stroke requirements for the other two DMs is a trickier to determine since it depends on the distribution of turbulence, and not just the turbulence strength. On the other hand, the stroke requirements are much lower and any commercial DM is likely to meet the requirement.

A simulation was run with the 3 DM MCAO system observing at a zenith angle of 45 degrees with an r_0 value of 0.08 m at zenith. The distribution of DM commands is plotted in Figure 8.
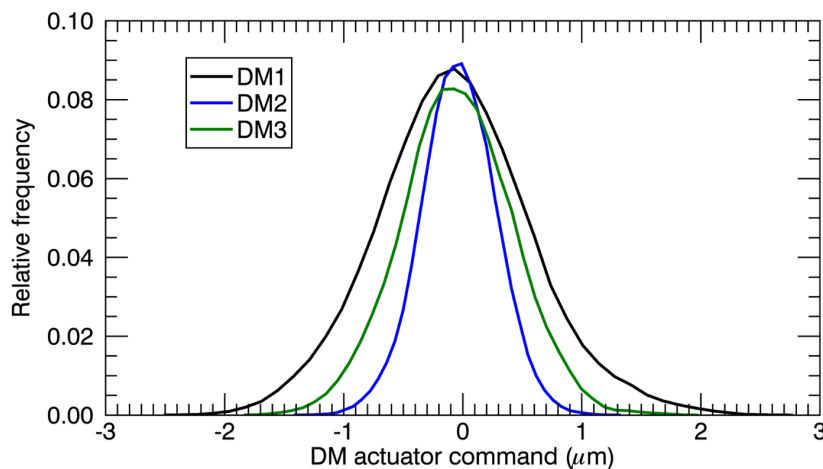
Figure 8: Histogram commands for DM1, DM2 and DM3

Based on these results, and adding some margin, we specify a minimum peak-to-valley stroke of 3 µm for DM2 and 4 µm for DM3.

4.4 DM order

The order in which the wavefront encounters the DMs has not yet been investigated. The "correct" way to order the DMs is to arrange them in the reverse order to the turbulence: from lowest altitude to highest altitude. Placing the DMs on this order reduces the effect of scintillation,[17] but scintillation is not a large term in the error budget. However, having the high altitude DMs between

---

[16]https://www.alpao.com/adaptive-optics/deformable-mirrors.html
[17]Flicker, Ralf C. "Sequence of phase correction in multiconjugate adaptive optics." Optics Letters 26.22 (2001): 1743-1745.

the ground-layer DMs and the WFS leads to a change in the registration between the DM and the WFS. Solar MCAO systems, which have small subapertures and DMs at a very high altitude, have had difficulty closing the AO loops due to this misregistration. If an ASM is in place, then the ground layer correction will occur first anyway.

GeMS corrects the turbulence in the opposite order: the order of the DMs is DM9, DM4.5 and DM0, where the number represents the conjugate altitude of the DM.

Currently, there are no AO simulation tools that include the effect of the pupil registration due to high altitude DMs. I am working on such a tool for the European Solar Telescope, but it is not yet in a state where I can produce results.

4.5 Other parameters

In Reference 1, it was found that neither the influence function of the actuators nor DM hysteresis play any role in the performance of GNAO.

The effect of dead actuators has yet to be evaluated and we consider it here. There are two common types of behavior for dead actuators. They are either "stuck" or "floating". Stuck actuators, as the name suggests, do not move. We will consider them stuck at the nominal flat position, although they could be stuck at any position. Floating actuators cannot be commanded but follow the behavior of their nearest neighbors. We will further assume that the location of the dead actuators is random and uncorrelated with the other dead actuators.

Simulations were run to evaluate the performance as a fraction of stuck actuators. The results, tabulated in Table 18, show that the location of the bad actuators, and not just their frequency, matters. The fraction of stuck actuators should be limited to less than 1%.

Percentage of stuck actuators	0	0.5%	1.0%	1.5%	2.0%	2.5%	3.0%
Mean K-band Strehl ratio	0.6900	0.6832	0.6793	0.6658	0.6714	0.6692	0.655

Table 18: Simulated average K-band Strehl ratio at zenith for the median turbulence profile as a function of percentage of stuck actuators.

5 Simulation results

End-to-end simulations were run in YAO to understand the performance of the proposed configuration. The same parameters were used as in the work presented in Reference 1 with the differences described in Section 2, as well as the following:

> 20x20 subapertures. Guide star locations [0,0] and [±35, ±35].
> DM1: 0 km, 21x21 actuators, 40 cm pitch
> DM2: 5 km, 19x19 actuators, 60 cm pitch
> DM3: 14 km, 19x19 actuators, 90 cm pitch

2500 iterations were run at 500 Hz for a total simulation time of 5 s. The simulation results using the median turbulence profile and varying the zenith angle are shown in Figure 9 and Table 19.
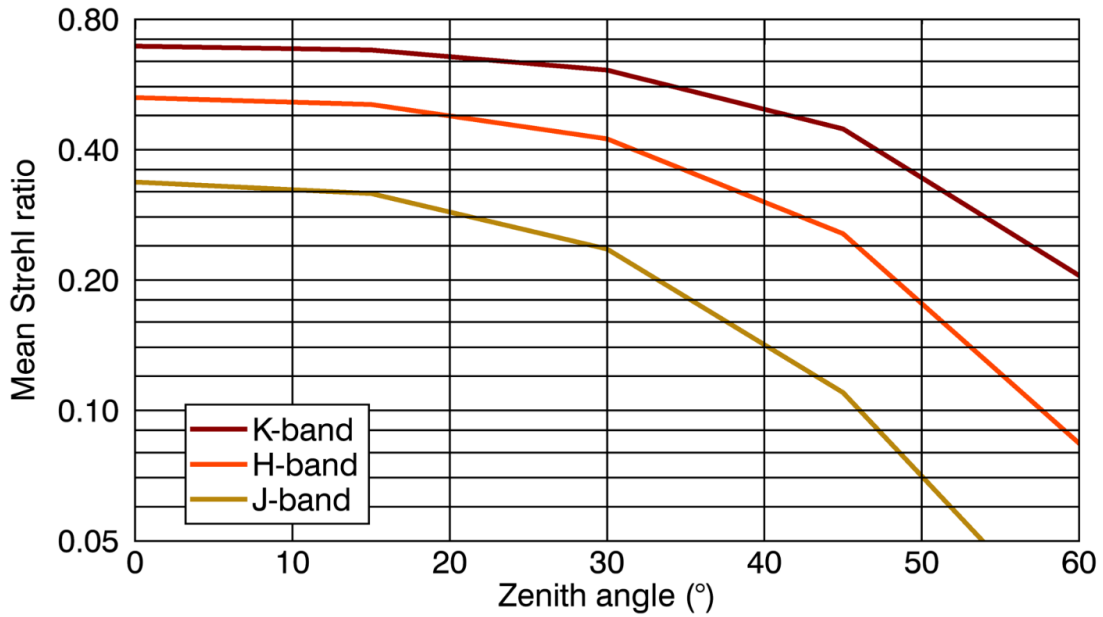
Figure 9: Simulated J-, H-, K-band Strehl ratio average for the median turbulence profile as a function of zenith angle.

Zenith angle	0º	15º	30º	45º	60º
J-band	0.337	0.317	0.236	0.110	0.029
H-band	0.528	0.509	0.424	0.256	0.084
K-band	0.694	0.680	0.611	0.447	0.205

Table 19: Simulated J-, H-, K-band Strehl ratio average for the median turbulence profile as a function of zenith angle.

The K-band Strehl and FWHM as a function of position on the field is plotted in Figures 10 and 11 respectively. The performance degradation at the top right hand corner is at least partially due to the location of the NGS guide stars.
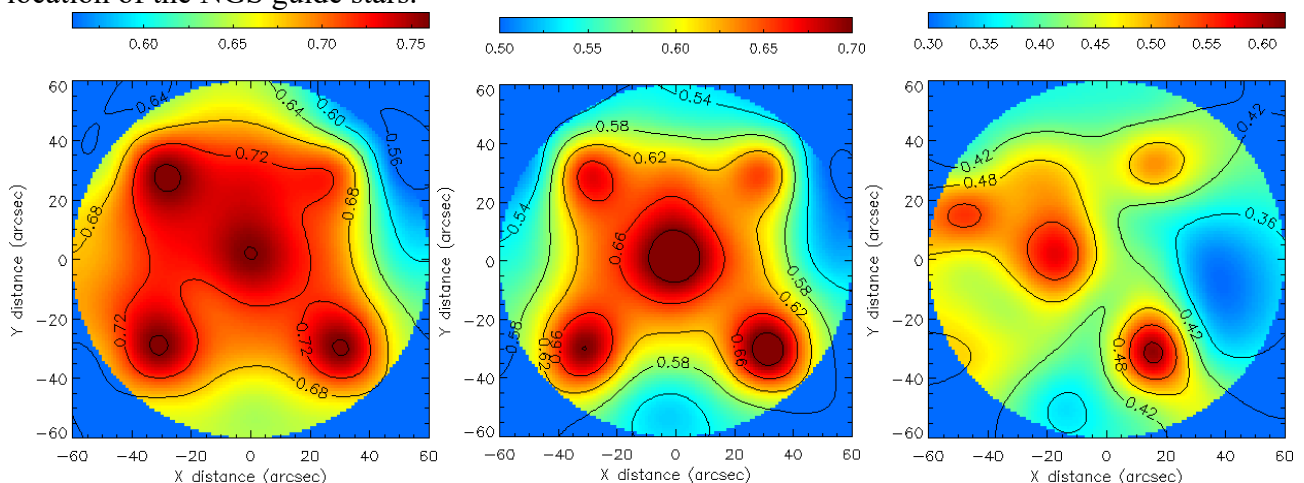
Figure 10: Variation in K-band Strehl ratio across the field for zenith angles 0°, 30° and 45°.
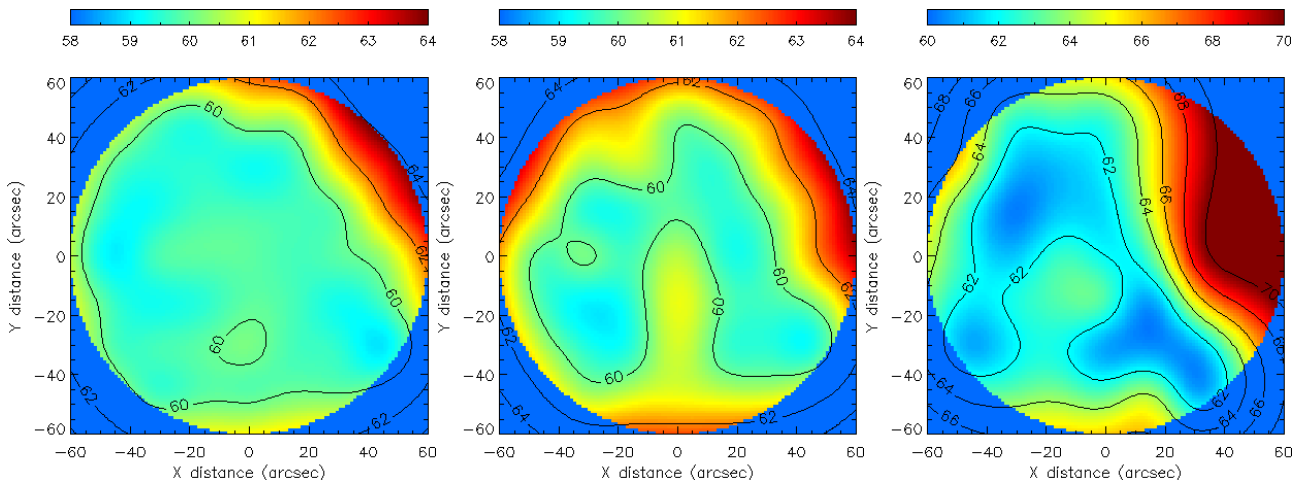
Figure 11: Variation in K-band FWHM across the field for zenith angles 0°, 30° and 45°.

Simulations using the median turbulence profile at zenith but varying the value of r_0 only (Figure 12 and Table 12).
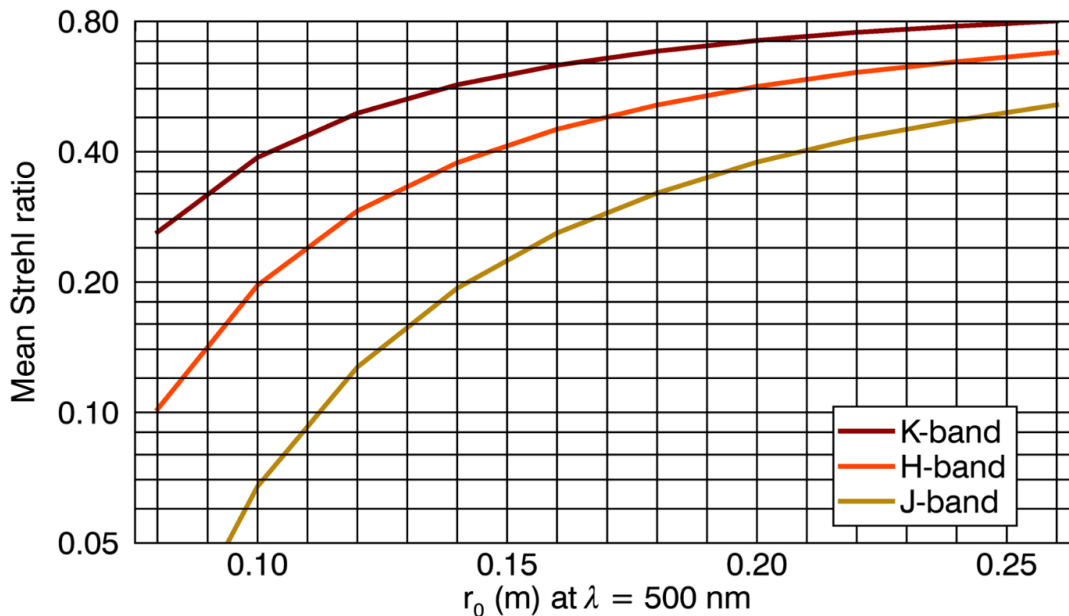
Figure 12: Simulated J-, H-, K-band Strehl ratio average for Configuration 3 for the median turbulence profile as a function of r_0.

r_0	0.08	0.10	0.12	0.14	0.16	0.18	0.20	0.22	0.24	0.26
J-band	0.0247	0.0675	0.1273	0.1937	0.2598	0.3211	0.3787	0.4296	0.4728	0.5133
H-band	0.1018	0.1966	0.2921	0.3775	0.4511	0.5129	0.5661	0.6103	0.6458	0.6782
K-band	0.2610	0.3881	0.4911	0.5712	0.6338	0.6829	0.7229	0.7549	0.7798	0.8021

Figure 13: Simulated J-, H-, K-band Strehl ratio average at zenith for the median turbulence profile as a function of r_0.

6 NGS wavefront sensor parameters

The NGS WFS consists of a focal plane array from which regions corresponding to the location of

the NGS are extracted, similar to the one implemented at Gemini South (called NGS2).[18] NGS2 reads three regions of interest in a 512x512 EMCCD with a plate scale of 0.235". This produces an approximately 120"x120" field of view. In this section, we investigate the performance as a function of plate scale.

6.1 Field of view

The field of view of the tip-tilt sensor must include the entire field of view passed to GNAO, which is a circle with a 2' diameter.

6.2 Plate scale and number of pixels

The optimal plate scale is a trade-off between maintaining a low measurement noise and adequately sampling the spot. For a Gaussian spot, we showed in Section 10 that a plate scale equal to the FWHM is adequate. However, the PSF at the focal plane will not be Gaussian, and simulations are needed to assess the impact of the plate scale on the performance.

Noiseless simulations were run to determine how the plate scale affects the performance. When observing at zenith in median seeing conditions, the simulated high-order wavefront correction is really good and there is a peak almost at the diffraction limit, as shown in Figure 14. To adequately sample this peak, very small pixels are required. However, the surrounding halo, which contains most of the energy, can be adequately sampled with a much larger plate scale.
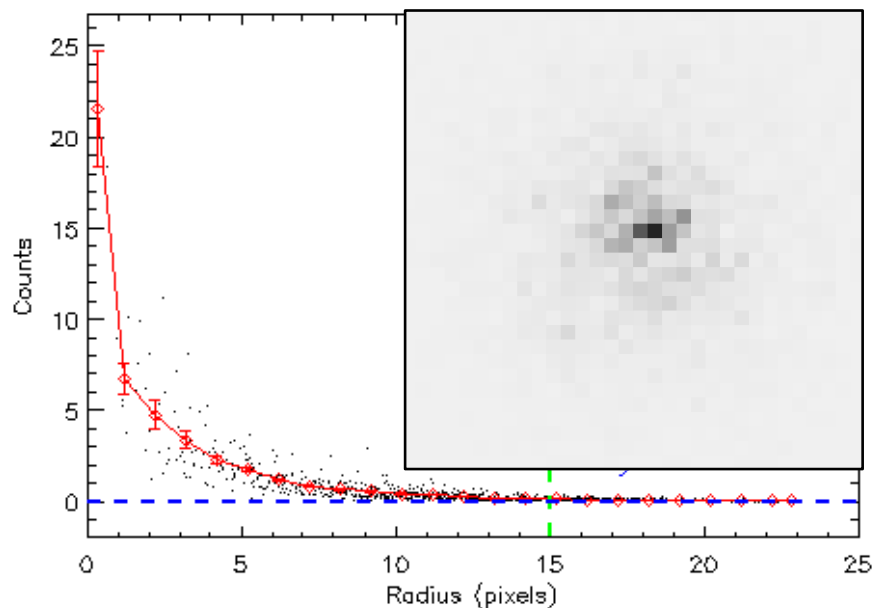
Figure 14: A typical NGS WFS image (inset) and its radial profile. The pixel scale is 25 mas.

The performance as a function of pixel size is plotted in Figure 15 with the centroid offsets to to [0", 0"] and [0.07", -0.03"]. When the Strehl ratio is very high, there is a modest degradation in performance with increasing plate scale. However, for lower (and probably more realistic) Strehl ratios, the plate scale does not play a large role.

---

[18]Rigaut, François, et al. "NGS2: a focal plane array upgrade for the GeMS multiple tip-tilt wavefront sensor." Adaptive Optics Systems V. Vol. 9909. International Society for Optics and Photonics, 2016.
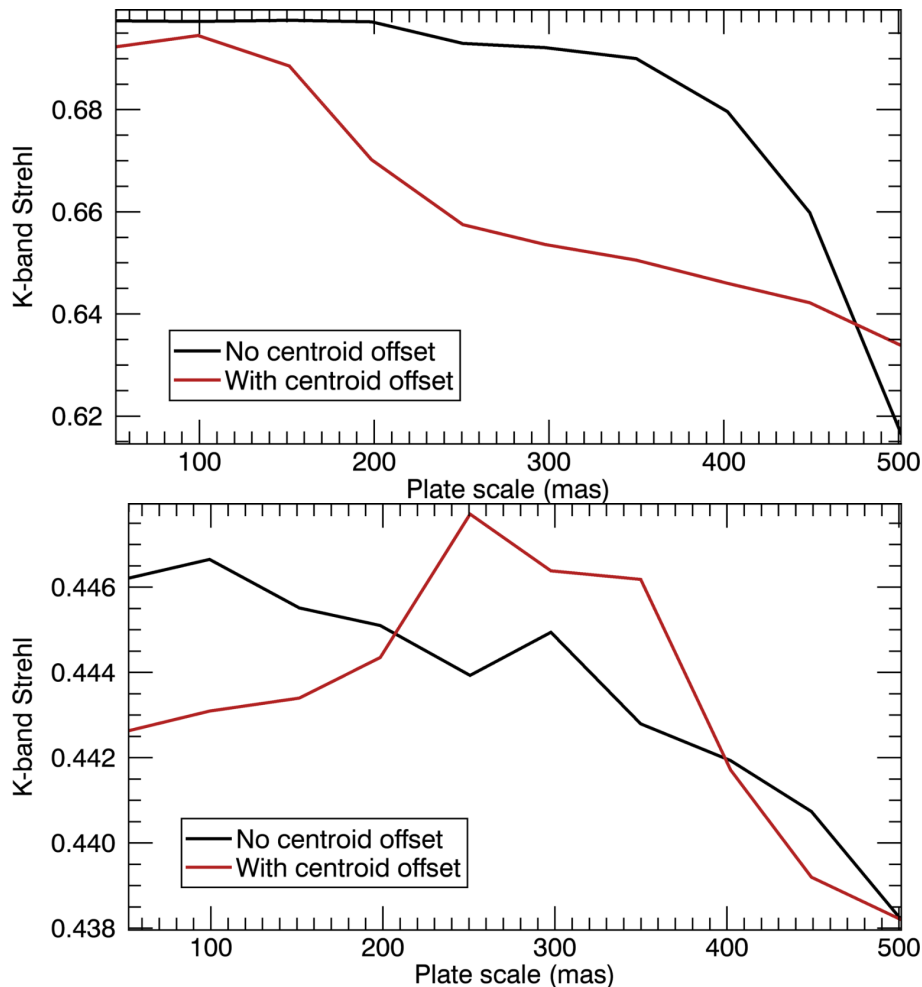
Figure 15: Simulated K-band Strehl ratio averaged over the whole field with and without a centroid offset at zenith (top) and at a zenith angle of 45° (bottom).

The other aspect to consider is the cosmetics of the camera. Where bad pixels are present, these can be replaced by an interpolation of the nearest neighbors without any loss of information (other than a slight increase in noise) if the spots are Nyquist sampled (2 pixels per FWHM). If there is a large number of bad pixels, then the spots need to be Nyquist sampled (say, 0.2"). If the number of bad pixels is very small, then we can avoid those regions where there are bad pixels, which allows us to increase the plate scale. We propose a plate scale of 0.35", with an acceptable range of 0.25" to 0.40". A detailed study is needed to trade-off the performance using bright NGSs on a very well corrected field with performance on fainter guide stars or when the Strehl ratio is lower. This value needs to be optimized based on the read out rate and noise characteristics of the camera.

The baseline is to read three stars but we have shown that where more stars are available, increasing the number of guide stars can reduce the tip-tilt anisoplanatic error. Therefore, it would be desirable to guide on up to six stars. While this might not be possible using the same technology as the NGS2 camera, sCMOS cameras are commercially available that may allow the read-out of the whole detector at full frame rate. For example, the Zyla 4.2 claims 80% QE and 1.1 e- read noise over an ROI of 512x512 pixels at 406 Hz, and 128x128 pixels at 1627 Hz. We would like something between those two values (e.g., 350x350 pixels at 600 Hz).

7 SFS wavefront sensor parameters

A slow focus sensor (SFS) is needed to measure focus due to changing sodium altitude, and other

low-order aberrations induced by the LGS elongation.[19] [20] These aberrations have been measured to be several hundred nanometers on the side-launched Keck II telescope, but do not appear to affect the image quality of the VLT's adaptive optics facility (AOF), which uses four side-launched lasers. The VLT has the benefit of sampling the spots adequately, and using four LGSs which could lead to the aberrations canceling on-axis. It is preferable to have the ability to measure LGS aberrations if they are present.

Focus and astigmatism can be measured by a 2x2 Shack-Hartmann WFS. To measure higher-order aberrations, we require more subapertures. We suggest a 5x5 Shack-Hartmann WFS in order to easily and quickly make the focus measurement using even the faintest guide stars. However, if a low read-noise camera is used (e.g., an EMCCD or a very low noise sCMOS device), then we should consider increasing the number of subapertures beyond this value.

As a comparison, the SFS at Keck Observatory, known as the low-bandwidth wavefront sensor (LBWFS) uses 20x20 subapertures (one-to-one match with the fast WFS) with 16x16 0.3" pixels per subaperture. It uses 20% of the light from the tip-tilt star. Because of the noisy characteristics of the camera they use, the LBWFS integration time can exceed 60s and cause operational inefficiencies on faint guide stars.

8 Summary

In this section, we summarize all of the parameters for convenience. Table 20 tabulated the parameters of the LGS WFSs, while Table 21 displays the DM parameters. An interesting idea to consider is the use of the ALPAO DM241 with 17x17 actuators as the ground-layer DM, which would eliminate the need for a tip-tilt mirror.

Parameter	Suggested value	Acceptable range
Subapertures	20x20	16x16 to 26x26
Pixels per subaperture	8x8	6x6 to 12x12
Plate scale	1"	0.8" to 1.2"
Field stop	8"x8" square	Depends on pixels

Table 20: Specification of LGS WFS parameters

---

[19] M. A. van Dam, A. H. Bouchez, D. Le Mignant and P. L. Wizinowich "Quasi-static aberrations induced by laserguide stars in adaptive optics," Opt. Express14, 7535-7540 (2006)

[20] Clare, Richard M., Marcos A. van Dam, and Antonin H. Bouchez. "Modeling low order aberrations in laser guide star adaptive optics systems." Optics express 15.8 (2007): 4711-4725.

Parameter	Suggested value	Acceptable range
DM1 altitude	0 km	
DM1 pitch	0.40 m	0.30 – 0.50 m
DM1 actuators across pupil	21	17 - 27
DM1 stroke	10 μm	≥8 μm
DM2 altitude	5 km	4.5 - 7 km
DM2 pitch	0.60 m	0.40 – 1.00 m
DM2 actuators across pupil	19	12 - 28
DM2 stroke	3 μm	≥2 μm
DM3 altitude	12 km	11-16 km
DM3 pitch	0.90 m	0.60 – 1.40 m
DM3 actuators across pupil	19	12 - 29
DM3 stroke	4 μm	≥3 μm

Table 21: Specification of DM parameters

Suggestions for the NGS WFS plate scale and number of pixels are tabulated in Table 22. The exact values will depend on the availability, read-out speed and noise characteristics of a suitable camera.

Parameter	Suggested value	Acceptable range
NGS plate scale	0.35"	0.25" - 0.40"
Pixels per subaperture	8x8	6x6 - 10x10
Number of pixels	343x343	300x300 - 480x480

Table 22: Specification of NGS WFS parameters

Table 23 presents suggested parameters for the SFS

Parameter	Suggested value	Acceptable range
Subapertures	5x5	2x2 - 10x10
SFS plate scale	0.3"	0.25" - 0.40"
Pixels per subaperture	10x10	8x8 - 16x16
Number of pixels	50x50	16x16 - 160x160

Table 23: Specification of SFS parameters

9 Appendices

9.1 Changes to simulations

In this section, we describe the differences between the system and the simulation parameters

corresponding the results presented here and those presented at the Conceptual Design Review and documented in "Simulated Performance of GNAO".[21] Following the Conceptual Design Review, three significant changes were made to the baseline architecture:

- the number of lasers was reduced from three to two
- the number of laser guide stars (LGSs) was increased from four to five (with a corresponding number of wavefront sensors (WFSs)
- the number of deformable mirrors (DMs) was increased from two to three

In addition to changes to MCAO system described above, one simulation parameter changed: the FWHM of the sodium layer increased from 8000 km to 12000 km, which is the typical value reported by Pfrommer.[22]

There was a bug in the parameter files which resulted in the high altitude DMs not having a sufficient number of actuators. The simulation and analytic computation results presented in Reference 21 have a lower Strehl ratio at the edges of the field than they should. This problem has been rectified for the simulations presented here.

9.2 LGS tomography

The LGS tomographic reconstructors are based on the original work by Ellerbroek et al.[23] These reconstructors have two steps: a tomography step, where the measurements from the 4-6 LGS WFSs are converted into a 3D wavefront estimate at the same resolution as the WFSs using a minimum-variance reconstructor, and a fitting step, which converts the 3D wavefront estimate into DM commands that minimize the wavefront error in the direction of the science targets. In this study, the wavefront was estimated at four altitudes: 0 km, 4 km, 8 km, and 16 km. Future work should investigate whether finer vertical and horizontal sampling, or adjusting the DM altitudes can improve the performance. In addition, the code could be rewritten to reduce the time it takes to compute the reconstructors.

9.3 NGS tomography

In this section, we describe how the tip-tilt tomography is performed. This approach is also documented in a very recent paper by van Dam et al.[24]

Without loss of generality, let us consider the the least-squares estimate of the on-axis tip-tilt, $\hat{a} = [\hat{a}_x, \hat{a}_y]$, given one or more tip-tilt measurements is given by:

$$\hat{a} = C_{as} C_{ss}^{-1} s = Ms$$

where $s = [[s_{1x}, s_{1y}], [s_{2x}, s_{2y}], \ldots, [s_{Nx}, s_{Ny}]]$ are the x and y tip-tilt measurements for stars 1, 2, …, N.[25][26] Matrix M is the reconstructor matrix, which relates how the 2N measurements relate to the tip-tilt estimate. The covariance matrices are calculated using the C_n^2 profile, the outer scale of turbulence and the telescope diameter, D (the calculations that follow assume a circular telescope with no central obscuration).

[21]Marcos van Dam, Gaetano Sivo and Eduardo Marin, "Simulated Performance of GNAO," v3.1: 22 October 2019
[22]T. Pfrommer and P. Hickson, "High-resolution lidar observations of mesospheric sodium and implications for adaptive optics," J. Opt. Soc. Am. A 27, A97-A105 (2010).
[23]Ellerbroek, Brent L. "Efficient computation of minimum-variance wave-front reconstructors with sparse matrix techniques." JOSA A 19.9 (2002): 1803-1816.
[24]Van Dam, Marcos A. et al, "Infrared tip-tilt sensing: on-sky experience, lessons learned and unsolved problems," AO4ELT6 (2019).
[25]D.T. Gavel, "NGAO real-time controller algorithms design document," v1.1a, (2009).
[26]R. Conan, "GMT LTAO – Tip-tilt tomography," V1.1 (2010)

In the noiseless case, the angular covariance matrix between two Zernike coefficients, $a_i(\theta_1)$ and $a_j(\theta_2)$ of two wavefronts from two sources at directions θ_1 and θ_2 is $\langle a_i(\theta_1)a_j(\theta_2)\rangle$. This can be evaluated using the very complicated expression first derived by Whiteley[27] and found in Conan.[26]

In this report, we use a direct calculation of the covariance matrices using numerical integration. The integrand is based on the filter function theory developed by Sasiela.[28] The numerical integration is carried out using the *qromo* routine in IDL. The results were found to be identical to those obtained using Whiteley's formulation.[29]

The evaluation makes use of the following relationship. Without loss of generality, we assume that one star is at [0,0]. If the second star is located at [θ,0], then:

$\langle a_2(0,0)a_2(\theta,0)\rangle = \langle a_2(0,0)a_2(0,0)\rangle - 0.5\langle(a_2(0,0) - a_2(\theta,0))^2\rangle$
$\langle a_2(0,0)a_3(\theta,0)\rangle = 0$
$\langle a_3(0,0)a_2(\theta,0)\rangle = 0$
$\langle a_3(0,0)a_3(\theta,0)\rangle = \langle a_3(0,0)a_3(0,0)\rangle - 0.5\langle(a_3(0,0) - a_3(\theta,0))^2\rangle$

The right hand side of the equations have two terms. The first term is the tip (or tilt) variance. The other terms are the parallel and perpendicular contributions to the anisokinetic error:

$$\langle(a_2(0,0) - a_2(\theta,0))^2\rangle$$
$$= \int_0^\infty dh \int_0^\infty dk 2\pi k \frac{0.0097 C_n^2(h)}{(k^2 + 1/L_0^2)^{11/6}} (\frac{4J_2(2\pi Rk)}{2\pi Rk})^2 [1 + 2J_1(2\pi k\theta h)$$
$$- 2J_0(2\pi k\theta h)]$$

and

$$\langle(a_3(0,0) - a_3(\theta,0))^2\rangle$$
$$= \int_0^\infty dh \int_0^\infty dk 2\pi k \frac{0.0097 C_n^2(h)}{(k^2 + 1/L_0^2)^{11/6}} (\frac{4J_2(2\pi Rk)}{2\pi Rk})^2 [1 - 2J_1(2\pi k\theta h)]$$

For small to modest offsets, the variance of the parallel component is three times the variance of the perpendicular component.

An integral in polar coordinates can be written as

$$\int_0^\infty dk 2\pi k$$

The integrands have three components:

$\frac{0.0097 C_n^2(h)}{(k^2 + 1/L_0^2)^{11/6}}$ is the filter function for the von Karman power spectrum.

$(\frac{4J_2(2\pi Rk)}{2\pi Rk})^2$ is the filter function for tip-tilt.

The third term is the anisoplanatic contribution in the parallel and perpendicular directions to the offset. The variance of the tip-tilt terms is obtained by removing the anisoplanatic filter function:

$\langle a_2(0,0)a_2(0,0)\rangle = \langle a_3(0,0)a_3(0,0)\rangle = \frac{1}{2}\int_0^\infty dh \int_0^\infty dk 2\pi k \frac{0.0097 C_n^2(h)}{(k^2 + 1/L_0^2)^{11/6}} (\frac{4J_2(2\pi Rk)}{2\pi Rk})^2$, where

the factor of half divides the total tip-tilt power into tip and tilt components. R is the radius of the telescope, and all the other symbols have their usual meaning.

For completeness, we state the total anisokinetic error here, which is merely the sum of the parallel and perpendicular components:

[27]M.R. Whiteley et al, "Temporal properties of the Zernike expansion coefficients of turbulence-induced phase aberrations for aperture and source motion," J. Opt. Soc. Am. A 15 (1998).
[28]R. Sasiela, "Electromagnetic wave propagation in turbulence," 2nd edition, SPIE Press (2007)
[29]R. Conan, personal communication (15 March 2011).

$$\sigma^2 = \int_0^\infty dh \int_0^\infty dk 2\pi k \frac{0.0097 C_n^2(h)}{(k^2 + 1/L_0^2)^{11/6}} \left(\frac{4J_2(2\pi Rk)}{2\pi Rk}\right)^2 [2 - 2J_0(2\pi k\theta h)]$$

To calculate the covariance when the star offsets are not aligned with either the tip or tilt offsets requires the coordinates to be transformed.

Once we have computed these covariance matrices, it is straight-forward to compute the tomographic error:
$\sigma^2 = trace(C_{aa} - C_{as}C_{ss}^{-1}C_{as}^T)$, or, in the case of noisy measurements with noise covariance matrix, C_{nn}:
$\sigma^2 = trace\left[C_{aa} - C_{as}(C_{ss} + C_{nn})^{-1}C_{as}^T\right]$.

This method is extended to calculate the tomographic tip-tilt error over a discrete number of points in the image plane. The tip-tilt command is the tip-tilt value that minimizes the error over the whole science field. The correction of the tip-tilt anisoplanatism modes should also use this approach, but currently does not. Instead, focus and astigmatism are added to the high-altitude DM (the so-called plate scale modes), with the reconstructor consisting of a least-squares inversion of the interaction matrix between the plate scale modes and the tip-tilt measurements on the NGS WFS.